

Manuscript Number: CRCHIMIE-D-15-00298R1

Title: Solid state NMR of salivary calculi: proline-rich salivary proteins, citrate, polysaccharide, lipid, and organic-mineral interactions

Article Type: Mémoire / Full paper

Keywords: Apatite, Citrate, Polysaccharides, Proline-rich proteins, REDOR, Salivary proteins, Statherin.

Corresponding Author: Dr. David Reid,

Corresponding Author's Institution:

First Author: Yang Li

Order of Authors: Yang Li; David Reid; Dominique Bazin; Michel Daudon; Melinda Duer

Manuscript Region of Origin: UNITED KINGDOM

Abstract: Solid state NMR (ssNMR) can characterize mineral (^{31}P) and organic (^{13}C) components of human salivary stones ($n = 8$). All show apatitic ^{31}P spectra. ^{13}C ssNMR indicates more protein, of more consistent composition, than apatitic uroliths, with signals from Tyr, Phe and His prominent. Citrate and lipid, identified by dipolar dephasing (DD), and polysaccharides are also observable in varying amounts. $^{13}\text{C}\{^{31}\text{P}\}$ rotational echo double resonance ($^{13}\text{C}\{^{31}\text{P}\}$ REDOR) identifies carbon atoms in close ($< \text{ca. } 0.5 \text{ nm}$) proximity to phosphorus and therefore probably binding with mineral. Citrate, sugar and carboxylate signals undergo strong $^{13}\text{C}\{^{31}\text{P}\}$ REDOR, also seen to signals between 50 and 60 ppm, from protein α -carbons and, possibly, phosphoserines and phospholipids, and sometimes to a 35 - 40 ppm envelope containing Asp- $\text{C}\alpha$ and Glu- $\text{C}\alpha$ signals. Amino acid analysis indicates high proline and aromatic content. ^{13}C ssNMR and amino acid composition is consistent with preponderance of proline-rich salivary proteins such as statherin.

Suggested Reviewers:

Opposed Reviewers:

Response to reviewers

Reviewer #1 We accept the reviewer's observations regarding the complexities of "crystallization inhibitors". We have accordingly altered the manuscript by:

- 1) Removing mention of "crystallization inhibitor" from the abstract, and
- 2) Considerably modifying the last paragraphs of Introduction, and Discussion.

We believe the conclusions of the paper are now actually stronger with these modifications.

Reviewer #2 We have corrected typographical errors including the one the reviewer alludes to specifically.

We have commented in the Materials and Methods on available sample and experiment durations.

1 **Solid state NMR of salivary calculi: proline-rich salivary proteins, citrate,**
2 **polysaccharide, lipid, and organic-mineral interactions.**
3

4
5
6
7 Yang Li^a, David G. Reid^a, Dominique Bazin^{b,c}, Michel Daudon^d, Melinda J. Duer^a
8
9

10
11
12 ^a Department of Chemistry, University of Cambridge, Lensfield Rd., Cambridge CB2 1EW,
13
14 UK.
15

16
17 ^b Laboratoire de Physique des Solides, CNRS, Université Paris-Sud, 91405 Orsay, France.
18

19 ^c Laboratoire de Chimie de la Matière Condensée de Paris Université Pierre et Marie Curie et
20
21 Collège de France, 11 place Marcelin Berthelot, 75231 Paris cedex 05, France.
22
23

24 ^d APHP, Hôpital Tenon, Service d'Explorations Fonctionnelles, 4 rue de la Chine, 75020
25
26 Paris, France.
27
28

29
30
31 Author for correspondence: Melinda J. Duer
32

33
34 Telephone: (+44)(0)1223-763934
35

36 Fax: (+44)(0)1223-336362
37

38 Email: mjd13@cam.ac.uk
39
40
41
42
43
44
45
46
47
48
49
50
51
52
53
54
55
56
57
58
59
60
61
62
63
64
65

Abstract

1
2
3
4
5 Solid state NMR (ssNMR) can characterize mineral (^{31}P) and organic (^{13}C) components of
6
7 human salivary stones (n = 8). All show apatitic ^{31}P spectra. ^{13}C ssNMR indicates more
8
9 protein, of more consistent composition, than apatitic uroliths, with signals from Tyr, Phe and
10
11 His prominent. Citrate and lipid, identified by dipolar dephasing (DD), and polysaccharides
12
13 are also observable in varying amounts. $^{13}\text{C}\{^{31}\text{P}\}$ rotational echo double resonance ($^{13}\text{C}\{^{31}\text{P}\}$
14
15 REDOR) identifies carbon atoms in close (< ca. 0.5 nm) proximity to phosphorus and
16
17 therefore probably binding with mineral. Citrate, sugar and carboxylate signals undergo
18
19 strong $^{13}\text{C}\{^{31}\text{P}\}$ REDOR, also seen to signals between 50 and 60 ppm, from protein α -
20
21 carbons and, possibly, phosphoserines and phospholipids, and sometimes to a 35 – 40 ppm
22
23 envelope containing Asp-C β and Glu-C γ signals. Amino acid analysis indicates high proline
24
25 and aromatic content. ^{13}C ssNMR and amino acid composition is consistent with
26
27 preponderance of proline-rich salivary proteins such as statherin.
28
29
30
31
32
33
34
35
36

37 **Keywords** Apatite, Citrate, Polysaccharides, Proline-rich proteins, REDOR, Salivary
38
39 proteins, Statherin.
40
41
42
43
44
45
46
47
48
49
50
51
52
53
54
55
56
57
58
59
60
61
62
63
64
65

1 Pathological calcification can occur at multiple anatomical sites and under a variety of
2 physiological conditions. The composition and structure of the resultant calcified materials
3 may provide clues to the pathological causes and molecular mechanisms leading to
4 calcification, and possibly suggest avenues for therapeutic intervention. Basic information on
5 the composition of these materials can be obtained with simple chemical analyses such as
6 determinations of elemental composition. However, information which may be critical to
7 identifying pathological causation, such as bio-mineral crystal structure, requires more
8 sophisticated physicochemical methodologies which provide structural information to
9 complement chemical analysis [1, 2].
10
11
12
13
14
15
16
17
18
19
20
21
22
23

24 X-ray diffraction is a powerful tool for defining the spatial arrangement of atoms in
25 crystalline or multi-crystallite materials. It can be used to determine the crystal structure, and
26 by comparison with published database “fingerprints” of chemically or synthetically well-
27 defined materials, chemical composition in favourable cases. It is widely used in
28 characterizing the crystalline components of biominerals including sialoliths [3-5]. Fourier
29 transform infrared spectroscopy (FTIR) can also be used to identify the structure and physical
30 phases of the material by probing the molecular vibrational modes which are functions of
31 molecular and crystal structures [6]. In pure organic phases, or mixed organic-inorganic
32 composites, the amide stretches due to backbone C-O and C-N of a peptide, for instance, give
33 distinctive IR spectra which can be related to backbone conformation. Common pathological
34 biomineral phases, such as calcium oxalate solvates and polymorphs widespread in kidney
35 stones, can be distinguished with zero-crossing-point first-derivative spectrophotometry [7],
36 and different apatite and other calcium phosphate materials can be identified by assigning P-
37 O stretches. Scanning electron microscopy (SEM) examines the surface of calcified material,
38 and is a useful method for characterizing crystallite morphology [8]. These important
39
40
41
42
43
44
45
46
47
48
49
50
51
52
53
54
55
56
57
58
59
60
61
62
63
64
65

1 physical methods, and others such as powder neutron diffraction (PND) and X-ray
2 fluorescence (XRF), have long been widely used to study many kinds of pathological
3 calcified materials, to determine molecular composition, and establish possible links between
4 structural and chemical properties and the etiopathogenesis of biomineralization [9].
5
6
7
8
9

10
11 Solid-state nuclear magnetic resonance spectroscopy (ssNMR) is widely used to study solid
12 material structures by virtue of its sensitivity to the local environment of each NMR receptive
13 atom [10]. Unlike X-ray scattering techniques, which rely on molecular crystallinity and long
14 range order for interpretable data, ssNMR (like FTIR) can effectively study materials such as
15 amorphous solids without long range order, and provide information from which local
16 structure can be inferred. In addition NMR data is often easier to interpret in terms of
17 molecular structure as each chemically unique atom gives rise to a single signal the frequency
18 of which directly depends, often in an interpretable way, on its chemical environment.
19 Considering the example of a protein, ^{13}C atoms in amino acids containing methyl groups
20 (Ala, Ile, Leu, Met, Val) will give rise to signals which are distinct from each other, and from
21 other sp^3 carbon atoms, which are distinct from aromatic carbons (His, Phe, Tyr, Trp), which
22 in turn are distinct from backbone and sidechain amide carbons, and acidic carboxylate
23 carbons. Similarly in phosphatic biominerals different phosphate environments, such as the
24 PO_4^{3-} groups in apatite give rise to different ^{31}P signals from HPO_4^{2-} in for instance brushite.
25 Under favourable circumstances NMR can yield complete atomic level molecular and even
26 crystal structures, although this is far from realized for complex mixtures such as pathological
27 calcifications. The potential of NMR in the study of the composition of renal calculi has been
28 demonstrated by Bak et al. [11] who distinguish from each other the common organic
29 (calcium oxalates, uric acid) and inorganic (apatite, struvite, brushite) constituents. Apatitic
30 stones in particular have also been shown by ssNMR to contain polysaccharides and proteins
31
32
33
34
35
36
37
38
39
40
41
42
43
44
45
46
47
48
49
50
51
52
53
54
55
56
57
58
59
60
61
62
63
64
65

1 of highly variable apparent composition [12] and citrate [13] in variable proportions. Using
2 the ssNMR technique REDOR atomic level (sub-nanometer) interactions between urolith
3 phosphates, and the polysaccharides, proteins and (when present) citrate, were also
4 demonstrated, prompting the suggestion that such interactions might reflect processes central
5 to urinary calculus biogenesis [12].
6
7
8
9
10

11
12
13
14 In this paper, we apply ssNMR to extend characterization of the composition of, and some
15 aspects of the mineral-organic interactions present in, salivary stones (sialoliths) [14, 15], to
16 our knowledge for the first time in these pathological materials. We show that this technique
17 constitutes a unique tool, complementary to the other techniques described above, to address
18 many aspects of the organic constituents of pathological calcifications. The necessary
19 background to the methods we use – cross polarization (CP), magic angle spinning (MAS)
20 and $^{13}\text{C}\{^{31}\text{P}\}$ REDOR [12], and dipolar dephasing (DD) [13] are described in the respective
21 references just cited. Amino acid analyses were also performed on four of the samples, and
22 the salivary protein statherin was identified as the most likely major organic component of
23 the stones, consistent with the signals observed in the ^{13}C ssNMR. The function of the
24 statherin is widely believed to be, at low concentrations, the inhibition of propagation of
25 calcium phosphate crystallization and crystal growth, exerted by binding strongly with the
26 nucleating mineral surface. However at high protein concentrations such proteins can
27 solidify and actually act as crystallization promoters *via* heterogeneous nucleation processes.
28
29
30
31
32
33
34
35
36
37
38
39
40
41
42
43
44
45
46
47
48
49
50
51
52
53
54
55
56
57
58
59
60
61
62
63
64
65

It is evidently the latter process which predominates in the stone materials we have studied.

Materials and methods

Eight sialoliths were from the Wharton's ducts of patients undergoing surgical sialolithotomy and they were initially examined by FTIR spectroscopy at the Hôpital Tenon, Paris. They were used in all analytical procedures with informed patient consent and institutional ethics approval.

Each one was studied using a stereomicroscope to define morphological type [16] and a Spectrospin Vector 22 Fourier transform infrared spectrometer (Bruker, Karlsruhe, Germany) to determine its mineral composition and detect the presence of protein and lipid [17].

All solid-state NMR measurements were performed on a Bruker 400 MHz Avance II spectrometer, at frequencies of 400.42, 162.1 and 100.6 MHz for ^1H , ^{31}P and ^{13}C respectively, using standard Bruker double and triple resonance magic angle spinning (MAS) probes. Samples were powdered using a pestle and mortar, packed into 4 mm zirconia rotors and spun at 12.5 kHz, except for the DD experiments where a spin rate of 6.25 kHz was used. Samples were characterized using cross-polarisation magic angle spinning (CP-MAS; ^1H 90° pulse length 2.5 μs , ^{31}P CP contact time 10 ms, ^1H - ^{13}C CP contact time 2.5 ms, spin lock field strength 70 kHz, SPINAL64 broadband decoupling at 100 kHz ^1H field, recycle time 2 s), DD (same ^1H - ^{13}C CP parameters, ^{13}C refocussing π -pulse at centre of DD period, DD time 100 μs) and REDOR (same ^1H - ^{13}C CP parameters, 10 ms dephasing time, interpulse spacing in ^{31}P π pulse train 80 μs synchronized with MAS period). ^{31}P and ^{13}C chemical shifts were externally referenced using commercial macrocrystalline HAp (Fluka) at a shift of 2.6 ppm relative to 85% phosphoric acid at 0 ppm, and the methylene signal of the α -polymorph of

glycine (Sigma) at 43.1 ppm relative to TMS at 0 ppm, respectively. Sample masses available for study varied between ca. 100, and only a few, milligrams; accordingly acquisition times for the most demanding experiment, the REDOR, varied from overnight, to three days, respectively. Other experiments could be correspondingly shorter, typically a few hours to overnight.

1
2
3
4
5
6
7
8
9
10
11
12
13
14
15
16
17
18
19
20
21
22
23
24
25
26
27
28
29
30
31
32
33
34
35
36
37
38
39
40
41
42
43
44
45
46
47
48
49
50
51
52
53
54
55
56
57
58
59
60
61
62
63
64
65

Results

We were able to carry out ssNMR on eight sialoliths. ^{31}P NMR confirms the apatitic nature of the stones and two spectra are overlaid in Figure 1. Some stones showed only a single signal at the chemical shift expected for pure HAp, broadened by environmental heterogeneity on account of the nanocrystalline nature of the mineral. Other stones showed distinct shoulders to low frequency of this apatite signal, the origin of which is unclear but which may reflect substitutions of minor cations (e.g. Mg^{2+}) and anions (e.g. CO_3^{2-}) into the calcium phosphate lattice, the presence of minor hydrogen phosphate species, and/or interactions with organic macromolecules [18]. Fig. 1 illustrates these two extremes. Fig. S1 in the online supporting information summarizes the ^{31}P data from all eight samples.

Typical ^{13}C spectra are shown in Fig. 2, along with some assignments of relevant signals to chemical functionalities; spectra from all eight samples are overlaid for comparison in online supporting information Fig. S2. The spectral intensities suggest organic material is much more abundant relative to mineral than is usual in apatitic kidney stones; it is also of a rather more uniform composition. While it is impossible to identify specific proteins or other biomacromolecules precisely by our ssNMR data, the spectra do provide some compositional information. In particular the unusually intense peaks (relative to the spectrum as a whole, and to a typical protein) between 110-160 ppm indicate that a high proportion of the proteins in these samples have abundant His, Phe and Tyr (and possibly Arg, signal at ca. 156 ppm) content. There is no sharp signal from the γ -carbon of collagen hydroxyproline at ca. 70 ppm, suggesting the proteins are not of collagenous origin.

1 Varying relative amounts of sugar signals are observed in all samples. These are the broad
2 peaks between ca. 65 and ca. 80 ppm due to the majority of the hydroxylated sugar carbons,
3
4 and the signal from sugar anomeric carbons at ca. 100 ppm which is particularly diagnostic of
5 sugars. The former, lower frequency spectral region also contains signals from citrate (the
6 quaternary 3-carbon signal at ca. 76 ppm) when it is observable. The overlapping sugar and
7 citrate signals can be distinguished by the DD procedure, which broadens the sugar signals
8 beyond detection due to ^{13}C - ^1H dipolar coupling with hydrogens directly attached to the
9 sugar carbons, while the citrate quaternary carbon, at 76 ppm, experiences no significant
10 change. The DD experiment also identifies signals from methyl groups and other mobile
11 protonated carbons because molecular motion serves to reduce the ^{13}C - ^1H dipolar coupling
12 which leads to signal loss. In particular the DD experiment highlights signals from
13 segmentally mobile lipids when they are present at observable levels. Finally this experiment
14 also highlights quaternary aromatic signals (e.g. His, Phe and Tyr C_γ , and Tyr C_ζ), and amide
15 (ca. 175 ppm) and carboxylate (shoulder at ca. 180 ppm) carbons. All these effects are
16 exemplified in Figure 3, and summarized for all eight stones in Figure S3 (online supporting
17 information).

18
19
20
21
22
23
24
25
26
27
28
29
30
31
32
33
34
35
36
37
38
39
40
41 The $^{13}\text{C}\{^{31}\text{P}\}$ REDOR experiment identifies signals from organic functionalities which are in
42 close proximity to phosphate ions, the bulk of which may be assumed to be in mineral
43 although there may be small contributions from organic phosphates such as phosphoserine.
44 The technique is thus a powerful tool for mapping organic functionalities in close proximity
45 to mineral, in effect within about 0.5 nm, and therefore likely involved in atomic length-scale
46 interactions with mineral atoms.

47
48
49
50
51
52
53
54
55
56 A typical REDOR experiment consists of two phases; in the first phase a reference spectrum
57 is obtained in which any through-space interaction between ^{13}C and ^{31}P is removed by the
58
59
60
61
62
63
64
65

1 MAS procedure, while in the second phase this interaction is restored by a series of
2 perturbing RF pulses applied at the ^{31}P resonance frequency. The REDOR effect manifests as
3 a reduction in intensity of signals from carbon atoms close to phosphorus atoms, in practice
4 within at most 1 nm, and is best appreciated by overlaying the reference spectrum and the
5 REDOR spectrum; typical examples are shown in Fig. 4, and all $^{13}\text{C}\{^{31}\text{P}\}$ REDOR data
6 summarized in Figure S4 (online supporting information). The REDOR experiment is a
7 powerful tool for mapping the organic functionalities in close proximity to mineral, and likely
8 involved in atomic length-scale binding with mineral atoms.
9

10
11
12
13
14
15
16
17
18
19
20
21
22 Where citrate is observable, it undergoes a strong $^{13}\text{C}\{^{31}\text{P}\}$ REDOR effect involving its
23 central C3 quaternary (76 ppm) and carboxylate (high frequency shoulder ca. 180 ppm)
24 carbons (the methylene carbons are obscured by protein signals) implying a strong binding
25 interaction with mineral, as observed in other calcified materials [19]. The broad sugar signal
26 envelope between ca. 70 and 80 ppm also shows $^{13}\text{C}\{^{31}\text{P}\}$ REDOR, as do some protein
27 signals, in particular the broad envelope of signals between ca. 50 and 60 ppm. In these
28 respects the $^{13}\text{C}\{^{31}\text{P}\}$ REDOR behaviour of the sialoliths resembles that previously reported
29 for apatitic uroliths [12]. Notes summarizing NMR data, and well as compositional
30 information from standard FTIR, for all sialoliths appears in the online supporting
31 information.
32
33
34
35
36
37
38
39
40
41
42
43
44
45
46
47
48
49
50
51
52
53
54
55
56
57
58
59
60
61
62
63
64
65

66 We were able to obtain amino acid content analyses for four of the samples using standard
67 amino acid analysis; the data are summarized in Table 1 and the raw data (duplicate
68 determinations for each sample) presented in Table S1 (online supporting information). Table
69 S1 shows that there is some variability in the measurements even within individual samples;
70 this is not surprising considering the powdered concretions are likely heterogeneous mixtures

1 of mineral, polysaccharides, small molecules including citrate and lipid, and undoubtedly
2 several different proteins. However there are some clear trends from the overall data. All
3
4 four stones show a high content of Glu/Gln, Gly, and, significantly, Pro, and (consistent with
5
6 the well resolved aromatic signals in the ssNMR), His, Phe, and Tyr. A protein database
7
8 similarity search detected matches with statherin with fair confidence (score of 115), and the
9
10 calculated amino acid compositions of statherin and its precursor peptide are compared with
11
12 mean amino acid contents of each of the four stones analysed, in Table 1. As mentioned, our
13
14 stone constituents are unlikely to represent a unique protein, but certainly proline-rich
15
16 salivary proteins, of which statherin is representative, are significantly present.
17
18
19
20
21
22
23
24
25
26
27
28
29
30
31
32
33
34
35
36
37
38
39
40
41
42
43
44
45
46
47
48
49
50
51
52
53
54
55
56
57
58
59
60
61
62
63
64
65

1
2
3
4
5 **Discussion**
6
7
8
9

10 Many sialoliths consist of an organic-rich core surrounded by concentric laminations of
11 alternating inorganic and organic materials [20]. The inorganic mineral phases are calcium
12 phosphates, usually hydroxyapatite, carbonated apatite (carbapatite), and the mineral
13 whitlockite (often containing some magnesium), and our samples are no exception. Reports
14 of the organic components imply much less consistency in composition. An early study
15 observed that the organic matrix forms a much higher proportion of salivary stones than it
16 does of urinary tract calculi [21], consistent with our observation, and contains proteins and
17 carbohydrates (galactose, glucose, mannose, rhamnose, fucose). Osuji and Rowland report
18 sugars, and protein rich in glycine, alanine, glutamate and aspartate, but devoid of collagen
19 (hydroxyproline) and keratin (cysteine) “marker” amino acids [22]. Basic proteins rich in
20 proline, glycine and glutamate/glutamine, are abundant in saliva [23, 24]. It is now clear that
21 saliva contains groups of unique proline-rich acidic and basic proteins, which may be
22 glycosylated [25, 26], proposed to act as inhibitors of calcium phosphate precipitation. They
23 may thus be important in maintaining calcium phosphate supersaturation and hence
24 protecting dental enamel, and might play an antibacterial role as well [27]. They include the
25 calcium binding seryl-phosphorylated polypeptide statherin [28]. A variety of ssNMR
26 methods have been used to study aspects of the interaction between statherin model peptides
27 and calcium phosphates [29], such as the orientation of the two N-terminal Phe rings of
28 adsorbed statherin relative to the surface of HAp [30, 31]. Using site specific ^{13}C labelling of
29 N-terminal acidic residues the importance of glutamates and aspartates in controlling
30 statherin binding to HAp surfaces has been demonstrated, using $^{13}\text{C}\{^{31}\text{P}\}$ REDOR methods
31
32
33
34
35
36
37
38
39
40
41
42
43
44
45
46
47
48
49
50
51
52
53
54
55
56
57
58
59
60
61
62
63
64
65

1 similar to those we report here [32]. Site-specific ^{13}C labelling of arginine and $^{13}\text{C}\{^{31}\text{P}\}$
2 REDOR [33], and ^{15}N labelling of lysine and $^{15}\text{N}\{^{31}\text{P}\}$ REDOR [34], demonstrate the
3 importance of basic, as well as acidic, groups in the statherin - HAp phosphates.
4
5
6

7
8
9 The organic phase of submandibular sialoliths can contain about 10% lipids by weight [35].
10 On the basis of lipid content and composition it has been proposed that proteolipids, and
11 calcium complexes with acidic phospholipids, probably derived from salivary gland
12 constituents, play a mechanistic role in the stone mineralization process [36]. High salivary
13 calcium, low salivary phytate (*myo*-inositol hexakisphosphate, a possible precipitation
14 inhibitor) and magnesium, but not pH and citrate, correlate with propensity towards
15 sialolithification [37]. Proteomic mass spectrometry detects peptides in submandibular
16 sialoliths consistent with the presence of members (e.g. the A chain of HNP-3) of the defensin
17 class of antibacterial proteins [38].
18
19
20
21
22
23
24
25
26
27
28
29
30
31

32
33 Citrate is abundant in bone and has been invoked as playing a role, not clear as yet, in orderly
34 biomineralization [19]. It also occurs commonly but not invariably in pathological apatitic
35 mineralizations besides sialoliths such as vascular calcifications and kidney stones [13]. Its
36 occurrence in the latter is interesting in view of the widespread use of oral potassium citrate
37 in urolithiasis prophylaxis [39]. The invariably strong $^{13}\text{C}\{^{31}\text{P}\}$ REDOR effect to citrate
38 (central C3 carbon, and carboxylate carbons) we observe in all the sialoliths in which citrate
39 is detectable by NMR implies a close atomic level association between citrate and mineral
40 which may be mechanistically significant in the sialolithiasis process in at least some
41 instances. As well as citrate, polysaccharide species are also intimately associated with HAp
42 in uroliths [12] and other pathological calcifications [40]. Similarly where polysaccharides
43 are detectable in our sialoliths $^{13}\text{C}\{^{31}\text{P}\}$ REDOR effects again provide evidence for strong
44
45
46
47
48
49
50
51
52
53
54
55
56
57
58
59
60
61
62
63
64
65

sugar-mineral association, which may be mechanistically significant.

In view of the detailed ssNMR studies published on the geometry of interactions between HAp and model statherin subsequences, and our findings that our sialoliths contain high proportions of salivary proteins typified by statherin, it is relevant to ask whether any of the $^{13}\text{C}\{^{31}\text{P}\}$ REDOR effects we observe are consistent with the proposed geometries. In the sialoliths the most consistently observed $^{13}\text{C}\{^{31}\text{P}\}$ REDOR effects are to the broad envelope of ^{13}C signals between ca. 50 and 60 ppm comprised of numerous overlapping signals from the α -carbon atoms of most of the amino acid types, as well as certain others such as the δ -carbons of Pro, and possibly from glyceryl and head group atoms of any phospholipids which may be present which will undergo strong intramolecular $^{13}\text{C}\{^{31}\text{P}\}$ REDOR effects. In some but not all stones there are also $^{13}\text{C}\{^{31}\text{P}\}$ REDOR effects to the 35 – 40 ppm spectral region which contains signals from Asp and Asn β - and Glu γ -carbons. Strong $^{13}\text{C}\{^{31}\text{P}\}$ REDOR effects to carboxylate groups (spectral region around 180 ppm) are particularly indicative of the involvement of acidic groups in the mineral structure but unfortunately it is impossible to distinguish effects to acidic amino acids (Asp, Glu) from those to citrate. There are no reliably discernible $^{13}\text{C}\{^{31}\text{P}\}$ REDOR effects to any of the aromatic signals between 110 – 160 ppm, including the signal at ca. 156 ppm from Tyr $\text{C}\zeta$ which may contain a contribution from Arg $\text{C}\zeta$. Statherin, and possibly other salivary proteins, is phosphorylated on some Ser residues; phosphoserine residues should undergo strong intraresidue $^{13}\text{C}\{^{31}\text{P}\}$ REDOR effects to $\text{C}\alpha$ (ca. 58 ppm) and $\text{C}\beta$ (ca. 65 ppm) [41] but again it is impossible to distinguish these (if any) from those to other protein and sugar signals. For such reasons of spectral overlap and signal degeneracy it is difficult to confirm that the detailed geometric models proposed for the statherin – apatite interaction are reproduced in our materials. It seems unlikely however that aromatic groups are located within 0.5 nm from the mineral.

1
2 In comparison with apatitic kidney stones, the protein content of sialoliths as reflected in ^{13}C
3
4 NMR is strikingly uniform although there is greater variation between stones in respect of the
5
6 less abundant sugars, citrate, and lipid (compare Fig. S2 which overlays the spectra of eight
7
8 sialoliths, with an overlay of ten apatitic urolith spectra in the online supplementary figure of
9
10 Reid et al. [13]). There is emerging consensus that the causative event in urolithiasis is the
11
12 occlusion of renal ducts by calcium phosphate crystals which eventually extrude into the
13
14 urinary space and nucleate further deposition of crystalline material, very commonly calcium
15
16 oxalates [42]. There is no generally accepted single causative event in the genesis of
17
18 sialoliths, although obstruction, low salivary flow rate, dehydration, changes in salivary pH,
19
20 epithelial cell debris, and bacterial infection, are all considered significant to the etiology
21
22 [43]. The high content of proline-rich salivary proteins in apatitic sialoliths is interesting in
23
24 view of the proposed role of at least some of them as inhibitors of calcium phosphate crystal
25
26 propagation. Whatever proteins solidify in sialolithiasis the low intensity of the $^{13}\text{C}\{^{31}\text{P}\}$
27
28 REDOR effects to protein signals suggests that the bulk of protein residues are not in atomic
29
30 length scale contact with mineral. In this respect they resemble the protein material in
31
32 uroliths in which $^{13}\text{C}\{^{31}\text{P}\}$ REDOR effects to protein are much less apparent than those to
33
34 polysaccharides and citrate [12]. In spite of intensive study of the protein content of
35
36 clinically significant kidney stones, which is dominated by inflammatory proteins, [44] there
37
38 is no corresponding data yet for the proteome of the tiny apatitic Randall's plaques believed
39
40 to represent the causative nidus of urolithic mineralization [45]. As such there is no
41
42 circumstantial or mechanistic evidence yet linking specific proteins (or other biomolecules)
43
44 with urolithogenesis.
45
46
47
48
49
50
51
52
53
54
55
56
57

58 The same is even more true of sialolithogenesis. The single published proteomics study
59
60
61
62
63
64
65

1 concentrated on the centre and periphery of the core, and was limited to stones in which these
2 structures were well developed and discernible [38]. In such cases the A chain of the
3 antibacterial defensin HNP-3 was identified using proteolytic fragment mass spectrometry.
4 The amino acid content of this peptide showed very low correspondence with our
5 experimental amino acid content measurements. Our studies examined the entire stone as it
6 was not possible to isolate core material specifically, so it is possible that defensin peptides
7 are present at low abundance and insignificant compared to the predominant proline-rich
8 salivary proteins we overwhelmingly find. It is not surprising that salivary proteins are major
9 constituents of sialoliths. At low concentrations these proteins are thought to inhibit
10 crystallization processes by binding to the growing faces of the crystallite nidus. At higher
11 concentrations they can solidify and promote calcium phosphate deposition by heterogeneous
12 nucleation. If our stones conform to the widely accepted model of sialoliths as an
13 amorphous mineralized core surrounded by concentric laminations of organic and inorganic
14 material [20] we might assume that the mineralization-inhibitory salivary proteins solidify
15 physically separated from mineral. This would be consistent with the comparatively
16 insignificant $^{13}\text{C}\{^{31}\text{P}\}$ REDOR effects unambiguously assignable to protein, relative to
17 citrate, signals. It may imply alternating episodes of deposition of mineral, and of
18 mineralization-inhibitory salivary proteins. Testing this will require isolation and study of
19 separate organic and mineral laminations in cases where this is possible. Another explanation
20 may be that proline-rich proteins aggregate and solidify under sialolithogenic conditions and
21 then accumulate solid calcium phosphate *via* the heterogeneous mechanisms alluded to
22 earlier. Under such circumstances protein-protein may predominate over protein-mineral
23 contacts, again consistent with the weak protein-mineral $^{13}\text{C}\{^{31}\text{P}\}$ REDOR effects. Future
24 work should be aimed at characterizing the sialolith proteome in more detail, and studying
25 the distribution and variation in composition of the protein content of stone core and
26
27
28
29
30
31
32
33
34
35
36
37
38
39
40
41
42
43
44
45
46
47
48
49
50
51
52
53
54
55
56
57
58
59
60
61
62
63
64
65

peripheral laminations. In this way a better understanding should be attained of the detailed mechanistic relationship between mineralization and mineral-organic composite formation leading to sialolithogenesis, and of treatments for prophylaxis.

1
2
3
4
5
6
7
8
9
10
11
12
13
14
15
16
17
18
19
20
21
22
23
24
25
26
27
28
29
30
31
32
33
34
35
36
37
38
39
40
41
42
43
44
45
46
47
48
49
50
51
52
53
54
55
56
57
58
59
60
61
62
63
64
65

1
2 **Conclusions**
3
4
5
6

7 1. We have applied ssNMR to extend characterization of the composition of, and some
8 aspects of the mineral-organic interactions present in, salivary stones (sialoliths), to our
9 knowledge for the first time in these pathological materials.
10
11

12 2. This technique represents a unique and complementary tool to address details of the
13 organic components in biocalcifications which may prove central to the mechanisms driving
14 pathological mineralization.
15
16

17 3. Indeed, we have identified different organic compounds in addition to the abundant
18 proteins, such as polysaccharides, lipids, and the high affinity calcium ligand citrate.
19
20

21 4. $^{13}\text{C}\{^{31}\text{P}\}$ rotational echo double resonance ($^{13}\text{C}\{^{31}\text{P}\}$ REDOR) indicates a degree of
22 binding between proteins and the mineral phase, probably related to the fact that some of
23 them (e.g. proline-rich salivary proteins such as statherin) are specific inhibitors of the
24 mineralization process.
25
26
27
28
29
30
31
32
33
34
35
36
37
38

39 Such approaches provide a unique opportunity to better understand the etiopathogenesis of
40 these calcifications, whereby ssNMR has significant potential in the characterization of
41 pathological biomineralization.
42
43
44
45
46
47
48
49
50
51
52
53
54
55
56
57
58
59
60
61
62
63
64
65

1
2 **Acknowledgements**
3
4
5
6

7 The U.K. EPSRC (Y. L.) and MRC (D. G. R.) for funding. We thank our colleague Peter
8
9 Sharratt in the Department of Biochemistry, University of Cambridge, for amino acid
10
11 analyses and protein database searching, and helpful discussions.
12
13
14
15
16
17
18
19
20
21
22
23
24
25
26
27
28
29
30
31
32
33
34
35
36
37
38
39
40
41
42
43
44
45
46
47
48
49
50
51
52
53
54
55
56
57
58
59
60
61
62
63
64
65

1
2
3 **References**
4
5
6

- 7 [1] D. Bazin, M. Daudon, C. Combes, C. Rey, *Chem. Rev.*, 112 (2012) 5092.
8
9 [2] J. Gomez-Morales, G. Falini, J.-M. Garcia-Ruiz, *Biological crystallization* (Eds.),
10 *Handbook of crystal growth*, 2015, p. 873.
11
12 [3] A. Teymoortash, P. Buck, H. Jepsen, J.A. Werner, *Arch. Oral Biol.*, 48 (2003) 233.
13
14 [4] O. Kasaboglu, N. Er, C. Tumer, M. Akkocaoglu, *J. Oral Maxil. Surg.*, 62 (2004) 1253.
15
16 [5] J.F. Sabot, M.P. Gustin, K. Delahougue, F. Faure, C. Machon, D.J. Hartmann, *Analyst*,
17 137 (2012) 2095.
18
19 [6] I. Faklaris, N. Bouropoulos, N.A. Vainos, *Cryst. Res. Technol.*, 48 (2013) 632.
20
21 [7] L. Maurice-Esteva, P. Levillain, B. Lacour, M. Daudon, *Clinica Chim. Acta*, 298
22 (2000) 1.
23
24 [8] C.B. Giray, M. Dogan, A. Akalin, J. Baltrusaitis, D.C.N. Chan, H.C.W. Skinner, A.U.
25 Dogan, *Scanning*, 29 (2007) 206.
26
27 [9] M. Daudon, P. Jungers, D. Bazin, *New Engl. J. Med.*, 359 (2008) 100.
28
29 [10] M.J. Duer, *Introduction to solid-state nmr spectroscopy*, Blackwell Science, Oxford,
30 2004.
31
32 [11] M. Bak, J.K. Thomsen, H.J. Jakobsen, S.E. Petersen, T.E. Petersen, N.C. Nielsen, *J.*
33 *Urol.*, 164 (2000) 856.
34
35 [12] D.G. Reid, G.J. Jackson, M.J. Duer, A.L. Rodgers, *J. Urol.*, 185 (2011) 725.
36
37 [13] D.G. Reid, M.J. Duer, G.E. Jackson, R.C. Murray, A.L. Rodgers, C.M. Shanahan,
38 *Calcified Tissue Int.*, 93 (2013) 253.
39
40 [14] J.D. Harrison, *Otolaryngol. Clin. N. Am.*, 42 (2009) 927.
41
42 [15] H. Iro, J. Długaiczek, J. Zenk, *Brit. J. Hosp. Med.*, 67 (2006) 24.
43
44
45
46
47
48
49
50
51
52
53
54
55
56
57
58
59
60
61
62
63
64
65

- 1
2
3
4
5
6
7
8
9
10
11
12
13
14
15
16
17
18
19
20
21
22
23
24
25
26
27
28
29
30
31
32
33
34
35
36
37
38
39
40
41
42
43
44
45
46
47
48
49
50
51
52
53
54
55
56
57
58
59
60
61
62
63
64
65
- [16] M. Daudon, C.A. Bader, P. Jungers, *Scanning Microscopy*, 7 (1993) 1081.
- [17] L. Estepa, M. Daudon, *Biospectroscopy*, 3 (1997) 347.
- [18] D. Bazin, C. Chappard, C. Combes, X. Carpentier, S. Rouzière, G. Andre, G. Matzen, M. Allix, D. Thiaudière, S. Reguer, P. Jungers, M. Daudon, *Osteoporosis Int.*, 20 (2009) 1065.
- [19] Y.Y. Hu, A. Rawal, K. Schmidt-Rohr, *Proc. Natl. Acad. Sci. U.S.A.*, 107 (2010) 22425.
- [20] S. Kraaij, K.H. Karagozoglou, T. Forouzanfar, E.C.I. Veerman, H.S. Brand, *Brit. Dent. J.*, 217 (2014) 1.
- [21] J.A. Harril, J.S.J. King, W.H. Boyce, *Laryngoscope*, 69 (1959) 481.
- [22] C.I. Osuoji, S.L. Rowles, *Calc. Tiss. Res.*, 16 (1974) 193.
- [23] M. Levine, P.J. Keller, *Arch. Oral Biol.*, 22 (1977) 37.
- [24] D.L. Kauffman, P.J. Keller, *Arch. Oral Biol.*, 24 (1979) 249.
- [25] R.S.C. Wong, A. Bennick, *J. Biol. Chem.*, 255 (1980) 5943.
- [26] A. Bennick, *Molec. Cell. Biochem.*, 45 (1982) 83.
- [27] D.I. Hay, A. Bennick, D.H. Schlesinger, K. Minaguchi, G. Madapallimattam, S.K. Schluckebier, *Biochem. J.*, 255 (1988) 15.
- [28] D.H. Schlesinger, D.I. Hay, *J. Biol. Chem.*, 252 (1977) 1689.
- [29] A. Roehrich, G. Drobny, *Acc. Chem. Res.*, 46 (2013) 2136.
- [30] T. Weidner, M. Dubey, N.F. Breen, J. Ash, J.E. Baio, C. Jaye, D.A. Fischer, G.P. Drobny, D.G. Castner, *J. Am. Chem. Soc.*, 134 (2012) 8750.
- [31] J.M. Gibson, J.M. Popham, V. Raghunathan, P.S. Stayton, G.P. Drobny, *J. Am. Chem. Soc.*, 128 (2006) 5364.
- [32] M. Ndao, J.T. Ash, N.F. Breen, G. Goobes, P.S. Stayton, G.P. Drobny, *Langmuir*, 25 (2009) 12136.

- 1
2
3
4
5
6
7
8
9
10
11
12
13
14
15
16
17
18
19
20
21
22
23
24
25
26
27
28
29
30
31
32
33
34
35
36
37
38
39
40
41
42
43
44
45
46
47
48
49
50
51
52
53
54
55
56
57
58
59
60
61
62
63
64
65
- [33] M. Ndao, J.T. Ash, P.S. Stayton, G.P. Drobny, *Surf. Sci.*, 604 (2010) L39.
- [34] J.M. Gibson, V. Raghunathan, J.M. Popham, P.S. Stayton, G.P. Drobny, *J. Am. Chem. Soc.*, 127 (2005) 9350.
- [35] B.L. Slomiany, V.L.N. Murty, M. Aono, A. Slomiany, I.D. Mandel, *Arch. Oral Biol.*, 27 (1982) 673.
- [36] A.L. Boskey, B.D. Boyansalyers, L.S. Burstein, I.D. Mandel, *Arch. Oral Biol.*, 26 (1981) 779.
- [37] F. Grases, C. Santiago, B.M. Simonet, A. Costa-Bauza, *Clinica Chim. Acta*, 334 (2003) 131.
- [38] J. Szalma, K. Böddi, E. Lempel, A.F. Sieroslawska, Z. Szabo, R. Harfouche, L. Olasz, A. Takatsky, A. Guttman, *Clin. Oral Invest.*, 17 (2013) 1709.
- [39] C.R. Tracy, M.S. Pearle, *Curr. Opin. Urol.*, 19 (2009) 200.
- [40] M.J. Duer, T. Friscic, D. Proudfoot, D.G. Reid, M. Schoppet, C.M. Shanahan, J.N. Skepper, E.R. Wise, *Arterioscler. Thromb. Vasc. Biol.*, 28 (2008) 2030.
- [41] L.P. McIntosh, H.S. Kang, M. Okon, M.L. Nelson, B.J. Graves, B. Brutscher, J. *Biomolec. NMR*, 43 (2009) 31.
- [42] S.R. Khan, B.K. Canales, *Urolithiasis*, 43 (2015) S109.
- [43] M. Escudier, Epidemiology and aetiology of salivary calculi, in: M. McGurk, J.G. Combes, (Eds.), *Controversies in the management of salivary gland disease*, Oxford University Press, 2013, p. 251.
- [44] B.K. Canales, L. Anderson, L. Higgins, K. Ensrud-Bowlin, K.P. Roberts, B.L. Wu, I.W. Kim, M. Monga, *Urology*, 76 (2010) 1017.e13.
- [45] A.P. Evan, E.M. Worcester, F.L. Coe, J. Williams, J.E. Lingeman, *Urolithiasis*, 43 (2015) S19.

1
2
3
4
5
6
7
8
9
10
11
12
13
14
15
16
17
18
19
20
21
22
23
24
25
26
27
28
29
30
31
32
33
34
35
36
37
38
39
40
41
42
43
44
45
46
47
48
49
50
51
52
53
54
55
56
57
58
59
60
61
62
63
64
65

Table 1 Amino acid composition (in mole percent) of four of the eight sialoliths studied.

Quoted values are means of two measurements; the corresponding raw data is shown in Table S1 (online supplementary information). N.B. the methodology does not quantify Cys or Trp. Calculated amino acid compositions of statherin and the statherin precursor peptide are also shown for comparison.

Amino acid	Sample				Model Protein	
	A	B	C	D	Statherin	Statherin precursor
Ala	2.7	2.9	3.6	5.0	0.0	4.8
Arg	7.8	7.7	8.1	7.0	7.0	4.8
Asp/Asn	5.4	5.1	6.1	9.3	2.3	1.6
Glu/Gln	15.1	15.4	14.1	10.6	16.3	11.3
Gly	9.8	9.3	9.5	10.4	7.0	4.8
His	5.9	4.6	7.4	8.5	9.3	8.1
Ile	3.3	3.8	3.4	3.3	2.3	4.8
Leu	5.3	5.6	5.0	6.6	4.7	8.1
Lys	4.1	3.9	4.9	6.0	2.3	3.2
Met	0.5	0.7	0.7	1.4	0.0	4.8
Phe	7.6	7.5	8.3	5.9	7.0	9.7
Pro	13.3	14.5	11.8	5.7	16.3	11.3
Ser	3.0	2.6	2.5	4.1	4.7	4.8
Thr	2.1	2.1	1.8	3.6	2.3	1.6
Tyr	10.5	10.6	9.2	6.6	16.3	11.3
Val	3.5	3.7	3.4	6.0	2.3	4.8

Figure Legends

1
2
3
4
5
6
7
8
9
10
11
12
13
14
15
16
17
18
19
20
21
22
23
24
25
26
27
28
29
30
31
32
33
34
35
36
37
38
39
40
41
42
43
44
45
46
47
48
49
50
51
52
53
54
55
56
57
58
59
60
61
62
63
64
65

Figure 1 Two representative ^{31}P sialolith spectra, one (sample C) showing no shoulders, the other (sample B) prominent shoulders (arrowed) to low frequency of the main apatite signal at ca. 2.6 ppm. All samples referred to throughout the paper are lettered (A, B etc.) alphabetically in the order in which they were received and anonymized.

Figure 2 Three typical ^{13}C spectra with key amino acids, sugars, citrate, and lipid, labelled. Note the variability of the citrate, sugar and lipid signal relative intensities.

Figure 3 Three typical ^{13}C dipolar dephased spectra showing protein amide, quaternary aromatic, and methyl, citrate and protein carboxylate, citrate C3, and lipid, non-dephasing signals.

Fig. 4 Typical $^{13}\text{C}\{^{31}\text{P}\}$ REDOR output from two stones. The entire $^{13}\text{C}\{^{31}\text{P}\}$ REDOR experiment is performed in two stages. First a reference ^{13}C spectrum is acquired in which the through space $^{13}\text{C} - ^{31}\text{P}$ nuclear magnetic dipole coupling is removed (by the magic angle spinning procedure), then a REDOR spectrum is acquired under circumstances (application of a series of MAS period-synchronized π RF pulses at the ^{31}P resonance frequency) which restore the $^{13}\text{C} - ^{31}\text{P}$ coupling, and broaden any signals from carbons close to phosphorus to the extent that they become undetectable. These signals are best identified by overlaying reference and $^{13}\text{C}\{^{31}\text{P}\}$ REDOR spectra; loss of intensity in the latter relative to the former is evidence of a $^{13}\text{C}\{^{31}\text{P}\}$ REDOR effect.

Figure 1
[Click here to download high resolution image](#)

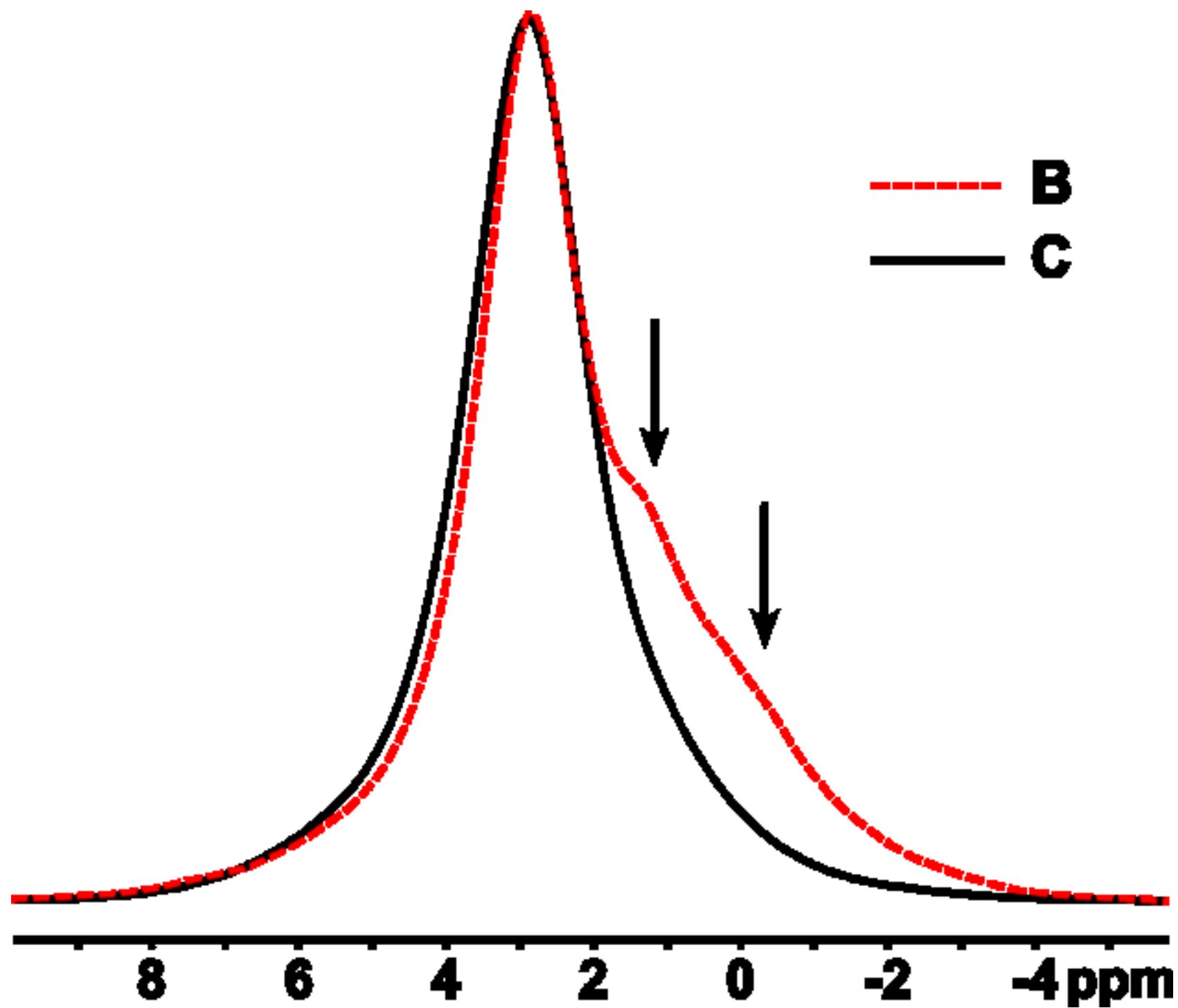


Figure 3
[Click here to download high resolution image](#)

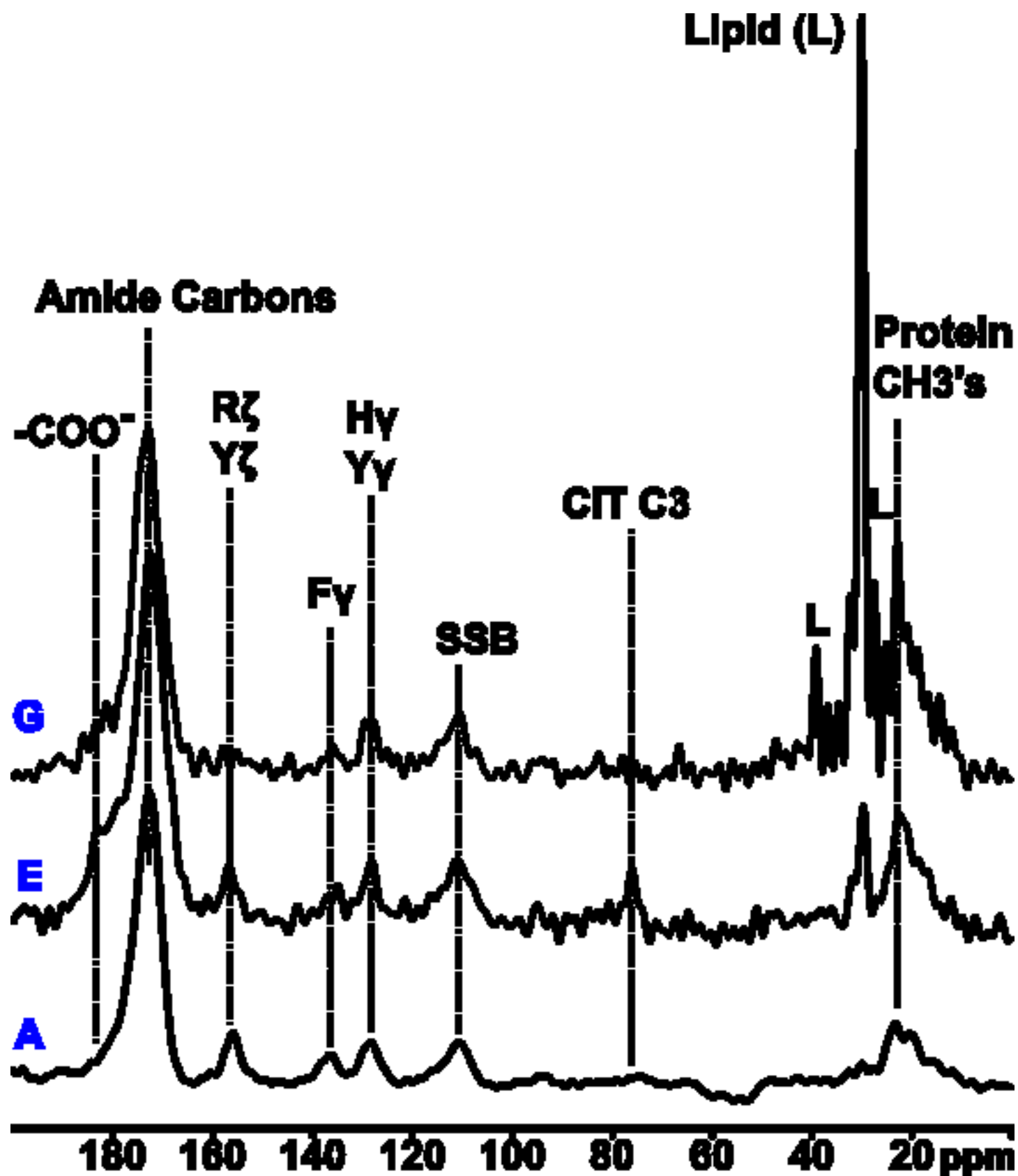
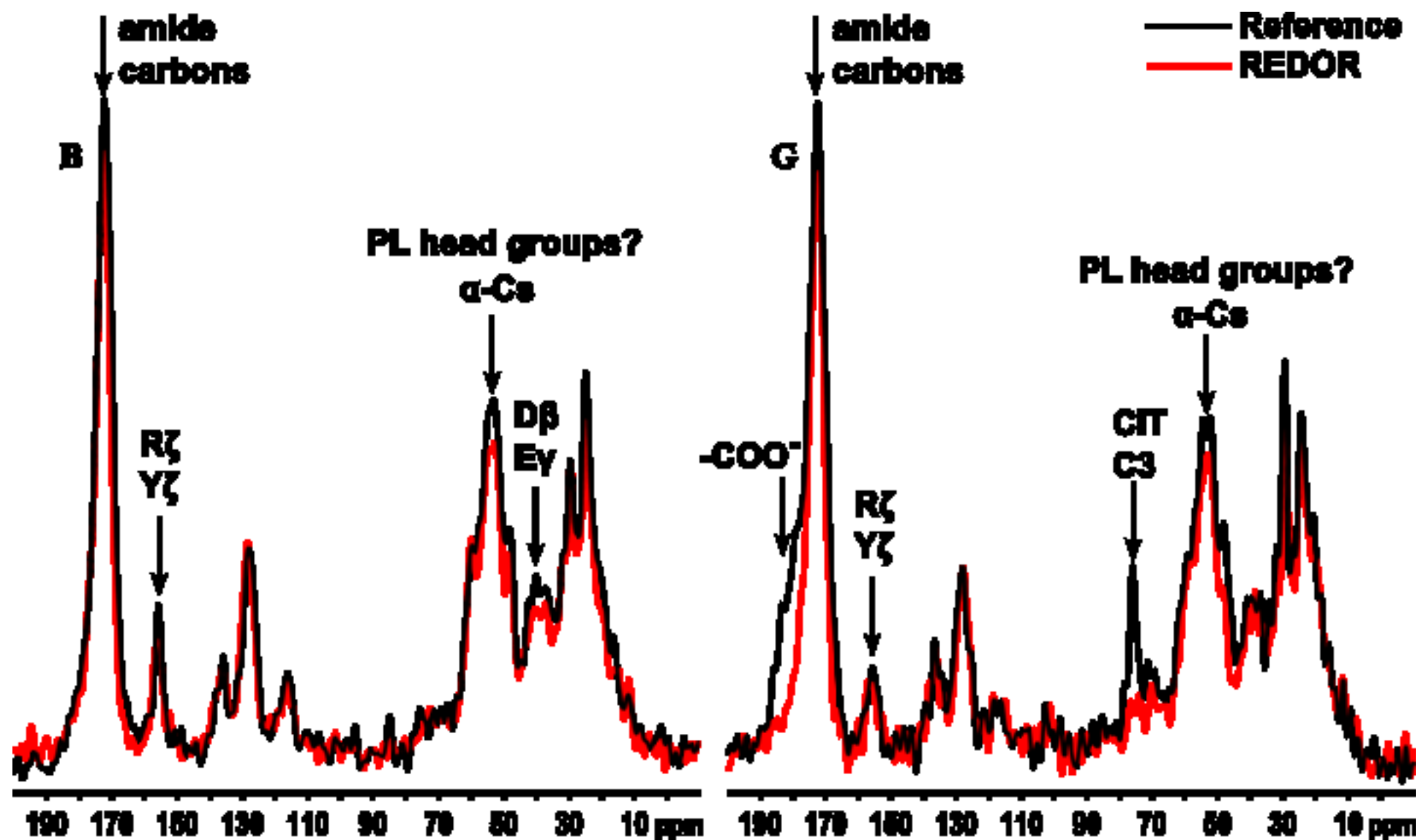


Figure 4
[Click here to download high resolution image](#)



Online supplementary information

[Click here to download Fichier média divers / e-component: Salivary stone NMR supporting information.pdf](#)